
A radiation-hydrodynamic model of accretion columns for ultra-luminous X-ray pulsars

Tomohisa KAWASHIMA^{1,*}, Shin MINESHIGE², Ken OHSUGA^{3,4}, AND TAKUMI OGAWA²

¹Center for Computational Astrophysics, National Astronomical Observatory of Japan, 2-21-1 Osawa, Mitaka, Tokyo 181-8588

²Department of Astronomy, Graduate School of Science, Kyoto University, Kitashirakawa, Oiwakecho, Sakyo-ku, Kyoto 606-8502

³Division of Theoretical Astronomy, National Astronomical Observatory of Japan, 2-21-1 Osawa, Mitaka, Tokyo 181-8588

⁴School of Physical Science, Graduate University of Advanced Study (SOKENDAI), Shonan Village, Hayama, Kanagawa 240-0193

*E-mail: kawashima@cfca.jp

Received (reception date); Accepted (acceptation date)

Abstract

Prompted by the recent discovery of pulsed emission from an ultra-luminous X-ray source, M82 X-2 (“ULX-pulsar”), we perform a two-dimensional radiation-hydrodynamic simulation of a super-critical accretion flow onto a neutron star through a narrow accretion column. We set an accretion column with a cone shape filled with tenuous gas with density of $10^{-4} \text{ g cm}^{-3}$ above a neutron star and solve the two dimensional gas motion and radiative transfer within the column. The side boundaries are set such that radiation can freely escape, while gas cannot. Since the initial gas layer is not in a hydrostatic balance, the column gas falls onto the neutron-star surface, thereby a shock being generated. As a result, the accretion column is composed of two regions: an upper, nearly free-fall region and a lower settling region, as was noted by Basko & Sunyaev (1976). The average accretion rate is very high; $\dot{M} \sim 10^{2-3} L_E/c^2$ (with L_E being the Eddington luminosity), and so radiation energy dominates over gas internal energy entirely within the column. Despite the high accretion rate, the radiation flux in the laboratory frame is kept barely below $L_E/(4\pi r^2)$ at a distance r in the settling region so that matter can slowly accrete. This adjustment is made possible, since large amount of photons produced via dissipation of kinetic energy of matter can escape through the side boundaries. The total luminosity can greatly exceed L_E by several orders of magnitude, whereas the apparent luminosity observed from the top of the column is much less. Due to such highly anisotropic radiation fields, observed flux should exhibit periodic variations with the rotation period, provided that the rotation and magnetic axes are misaligned.

Key words: accretion, accretion disks — hydrodynamics — radiation: dynamics — stars: neutron

1 Introduction

The discovery of pulsed emission from the representative Ultra-luminous X-ray sources (ULX), M82 X-2, by Bachetti et al.

(2014) was really sensational, since it for the first time provided good piece of information regarding the mass of the central objects in the ULXs. The ULXs are off-nuclear, compact,

very luminous X-ray sources with X-ray luminosities exceeding $\sim 10^{39}$ erg s $^{-1}$ (see reviews by Fabbiano 1989; Soria 2007; Feng & Soria 2011). There has been a long debate regarding the central engine of the ULXs: it could be either sub-critical accretion onto an intermediate-mass black hole (see e.g., Colbert & Mushotzky 1999; Makishima et al. 2000), or super-critical accretion onto a normal stellar-mass black hole (see e.g., King et al. 2001; Watarai et al. 2001; Vierdayanti et al. 2006), or the combination of these two. Although the direct mass measurement is the most effective way to settle down this issue, it is not always feasible due mainly to technical difficulties. In fact, ULXs are mostly very faint because of large distances. That is, there had been no direct evidences in favor of or against the super-critical accretion scenario for ULXs until the discovery of the ULX-pulsar. Since it is obvious that the mass of a neutron star (NS) is less than $\sim 2 M_{\odot}$, the discovery of the ULX-pulsar robustly points to the occurrence of super-critical accretion, at least, in some ULXs. (We cannot ruled out a possibility that the ULXs may be a heterogeneous group.)

The discovery of the ULX-pulsar has re-opened the issue of super-critical accretion onto a magnetized NS. This is not totally a new issue but was already intensively discussed in the 1970's, being pioneered by (Basko & Sunyaev 1976, hereafter, BS76). They solved one-dimensional structure of an accretion column, finding that the column is composed of two regions: an upper, nearly free-fall region and a lower settling region. They also claimed luminosities can naturally exceed the Eddington luminosity, since copious photons produced via dissipation of kinetic energy of accreting gas propagate towards side boundaries and can freely escape. Large amounts of photons can thus leak away from the side of the column. BS76 mainly addressed the super-critical accretion problem assuming hollow columns, and the limiting luminosity sensitively depends on the geometry of the accretion funnel, i.e., the thickness parameter of the wall of the column. The two dimensional gas motion was not taken into account, and the super-critical column accretion without assuming the hollow structure is not well understood. In addition, they assumed a radiative diffusion approximation to evaluate radiative flux at the side surface of the accretion column, which may underestimate the amount of the photons escaping from the side wall of the column.

In this *letter*, we mainly address the following questions: (1) How is super-critical accretion through a narrow accretion column on a star feasible? (2) Can the luminosity of the ULX-pulsar be explained? (3) What observational signatures are expected for such a source? (4) Are there any substantial differences between the accretion processes onto black holes and those onto NSs? In relation to these questions, it is of great importance to note that Ohsuga (2007) solved the problem of super-critical accretion disk onto non-magnetized NSs for the first time, by means of the two-dimensional radiation-

hydrodynamic (RHD) simulations. His main conclusions are that (1) super-critical accretion is indeed feasible and that (2) a large fraction of the liberated energy goes to kinetic energy in NS accretion. By contrast, more fraction of energy goes to radiation in black hole accretion. In the case of accretion onto strongly magnetized NSs, however, flow structure is distinct from that onto non-magnetized NSs: the strong magnetic fields of the NSs penetrating the accretion disks can disrupt the disk accretion and polar accretion flows aligned with the B-fields of the NSs can be formed inside Alfvén radii.

To examine whether the situation changes or not in the case of column accretion, we solve the gas dynamics and radiation transfer inside the funnel by two-dimensional RHD simulations. We expect much larger radiation output from the side wall than that from the top of accretion column, thus very high accretion luminosities being expected. Such geometrical differences will be essential from the viewpoints of radiation hydrodynamics, as will be demonstrated in this *letter*.

2 Our Model and Numerical Methods

We apply the simulation by Ohsuga (2007) to the case of NS accretion through a narrow accretion column (or funnel). We set a calculation box with a cone shape having a half opening angle of $\pi/6$ on the NS surface and fill it with uniform tenuous gas with density of $\rho = 10^{-4}$ g cm $^{-3}$ and high temperature of $T_{\text{gas}} = 10^7$ K. We further assume that the initial radiation temperature surrounding the column is low, $T_{\text{rad}} = 10^4$ K, and that gas has no angular momentum, for simplicity. The mass of a NS is set to be $M = 1.4 M_{\odot}$.

Since the gas layer within the column is not in hydrostatic balance, gas starts to fall onto the lower boundary after the start of a simulation. We calculate two dimensional gas motion and radiation transfer by solving a set of RHD equations in the spherical coordinates (r, θ, φ) , assuming axisymmetry. The basic equations are

$$\frac{\partial \rho}{\partial t} + \nabla \cdot (\rho \mathbf{v}) = 0, \quad (1)$$

$$\frac{\partial(\rho v_r)}{\partial t} + \nabla \cdot (\rho v_r \mathbf{v}) = -\frac{\partial p}{\partial r} + \rho \left[\frac{v_{\theta}^2}{r} - \frac{GM}{(r-r_s)^2} \right] + \frac{\chi}{c} F_0^r, \quad (2)$$

$$\frac{\partial(\rho r v_{\theta})}{\partial t} + \nabla \cdot (\rho r v_{\theta} \mathbf{v}) = -\frac{\partial p}{\partial \theta} + r \frac{\chi}{c} F_0^{\theta}, \quad (3)$$

$$\frac{\partial e}{\partial t} + \nabla \cdot (e \mathbf{v}) = -p \nabla \cdot \mathbf{v} - 4\pi \kappa B + c \kappa E_0, \quad (4)$$

$$\frac{\partial E_0}{\partial t} + \nabla \cdot (E_0 \mathbf{v}) = -\nabla \cdot \mathbf{F}_0 - \nabla \mathbf{v} : \mathbf{P}_0 + 4\pi \kappa B - c \kappa E_0. \quad (5)$$

Here, ρ is the mass density, $\mathbf{v} = (v_r, v_{\theta}, v_{\varphi})$ is the velocity (we set $v_{\varphi} = 0$, assuming no angular momentum of gas), p is the gas pressure, e is the internal energy density of gas, B is the blackbody intensity, E_0 is the radiation energy density of gas, $\mathbf{F}_0 = (F_0^r, F_0^{\theta})$ is the radiative flux, \mathbf{P}_0 is the radiation

pressure tensor (all of the quantities with suffix 0 are measured in the comoving frame of the fluid), κ is the absorption opacity, and $\chi = \kappa + \rho\sigma_T/m_p$ is the total opacity, where σ_T is the cross section of Thomson scattering and m_p is the proton mass. We do not take into account thermal Compton cooling/heating, which, if included, might change the temperature structure near the NS surface, though the overall structure should not alter significantly because of a very large optical depth of the column. General relativistic effects are incorporated by a pseudo-Newtonian potential prescribed by Paczyński & Wiita (1980), $\Psi = -GM/(r - r_s)$. Here, $r_s (= 2GM/c^2)$ is the Schwarzschild radius, G is the gravitational constant, and c is the speed of light. Simulations are carried out using a RHD code (Ohsuga et al. 2005; Ohsuga 2007), which solves the radiative transfer by adopting the flux-limited diffusion (FLD) approximation (Levermore & Pomraning 1981; Turner & Stone 2001) and hydrodynamic equations by using Virginia Hydrodynamics One (VH-1) based on Lagrange-remap version of the piecewise parabolic method (PPM, Colella & Woodward 1984), which is the third order Godunov's scheme.

The size of the computational domain is $r_{\text{in}} \leq r \leq r_{\text{out}}$ and $\theta_{\text{in}} \leq \theta \leq \theta_{\text{out}}$, where $(r_{\text{in}}, r_{\text{out}}) = (2.4r_s, 500r_s)$ and $(\theta_{\text{in}}, \theta_{\text{out}}) = (0, \pi/6)$; that is, we set $r_{\text{in}} \sim 10$ km, typical NS radius. We set a rather long accretion column (with a height of $500 r_s$) so as to include the trapping radius, which is expected to be at $r \sim (L/L_E)r_s$ (Begelman 1978), within the calculation box. (We will show later $L/L_E \sim 10^2$.) However, we focus our discussion in a narrow region, within 40 km ($\sim 10r_s$).

The number of grid cells is $N_r \times N_\theta = 288 \times 96$. The grid points are distributed such that $\Delta \log r = (\log r_{\text{out}} - \log r_{\text{in}})/N_r$ and $\Delta \theta = 1/N_\theta$.

At $r = r_{\text{in}}$ the accreting gas is absorbed, however, we assume that the energy carried by the gas is immediately converted to the radiation and is released as outgoing radiation flux (Ohsuga 2007). The top of the computation box at $r = r_{\text{out}}$ is set to be a free boundary, where both inflow and outflow of gas is allowed, i.e., the fluid quantities with no gradient are assigned to the ghost cells at every time step. We impose the mirror boundary condition both at $\theta = \theta_{\text{in}}$ and θ_{out} for the gas. As for the radiation, we set the mirror boundary at $\theta = \theta_{\text{in}}$, while we let radiation go out through the boundary at $\theta = \theta_{\text{out}}$ with radiation flux, $F_0^\theta = cE_0$.

We set the initial mass density to be $\rho = 10^{-4} \text{ g cm}^{-3}$ so as to reproduce the luminosity of M82 X-2, $L \sim 10^2 L_E$ for neutron stars with $1.4M_\odot$, i.e., $\dot{M} \sim 10^{20} \text{ g s}^{-1}$. Here, we have assumed the radiative efficiency ~ 0.1 . By using the relation $\dot{M} \simeq 4\pi r^2 \rho v_{\text{ff}} (\Omega/4\pi)$, we can obtain $\rho \sim 10^{-4} \text{ g cm}^{-3}$ for a radius inside which matter can accrete enough by the end of our simulation $r \sim 5 \times 10^7 \text{ cm}$, free-fall velocity there $v_{\text{ff}} \sim 3 \times 10^8 \text{ cm s}^{-1}$, and the solid angle subtended by the accretion column $\Omega \sim 0.1 \times (4\pi)$. In fact, we confirm that the sim-

ulated luminosity is $\sim 10^{40} \text{ erg s}^{-1}$, which is consistent with the estimated luminosity of M82 X-2.

3 Results

As was mentioned before, gas starts to freely fall towards the NS immediately after a simulation starts, since there is no sufficient pressure force preventing the gas fall in the initial state. The mass accretion rate onto the NS shows $\sim 10^{2-3} L_E/c^2$, as expected above.

We first show snapshots displaying gas and radiation properties over the two-dimensional plane in figure 1. These are color contours of matter density overlaid with gas velocity [panels (a) and (c)] and those of radiation energy density overlaid with comoving radiation flux [panels (b) and (d)], respectively. The right two panels are magnified views of the innermost parts of the corresponding left panels.

Two-zone structure is very clear in these plots. The interface between the two zones is located at around $r = 13 \text{ km} \equiv r_{\text{shock}}$, where a shock structure is observed there; velocity vectors are uniformly downward in the upper free-fall region, whereas they show significant deviations from the uniform down-flow below the interface. Even circular motion is observed there.

Another important feature found in this figure is that most of radiation originates from the side wall of the lower settling region of the accretion column, not from the top of the column. Interestingly, the luminosity of the NS surface is kept barely below $L_E \times \Omega/(4\pi)$ so that mass accretion onto the NS can proceed, liberating accretion energy sideways. The inset figure in panel (d) of figure 1 clearly shows that the radiation flux profile $F_{\text{side}} \equiv F_0^\theta(r, \theta_{\text{out}})$ is nearly flat along the side wall below the interface. We see that the fractional luminosity $F_{\text{side}} \Delta S$ exceeds the Eddington luminosity ($\simeq 2 \times 10^{38} \text{ erg s}^{-1}$) at $r < r_{\text{shock}}$, where $\Delta S \equiv 2\pi r \sin \theta \Delta r$ with Δr being the mesh spacing ($\Delta r \approx 0.2 \text{ km}$ near the NS surface). The total luminosity amounts to $L \sim 6 \times 10^{40} \text{ erg s}^{-1} \sim 300 L_E$, as will be explicitly shown later.

In order to check how physical quantities vary as matter falls in the settling region, we plot the azimuthally averaged gas density and velocity in figure 2. We find that matter density gradually increases downward by about two orders of magnitudes, while the absolute value of gas velocity decreases downward by roughly the same orders of magnitudes. These gradual changes arise, since we azimuthally averaged the physical quantities, and since the shock surface is not parallel to NS surface but is tilted (see figure 1). Note also that the radiation entropy displayed in the bottom panel shows a hump with a plateau shape below the shock region, indicating that energy dissipation really occurs there and that dissipated energy directly goes to radiation with going very little to gas. (Note that the gas entropy is very small, compared with the radiation entropy.) The plateau shape

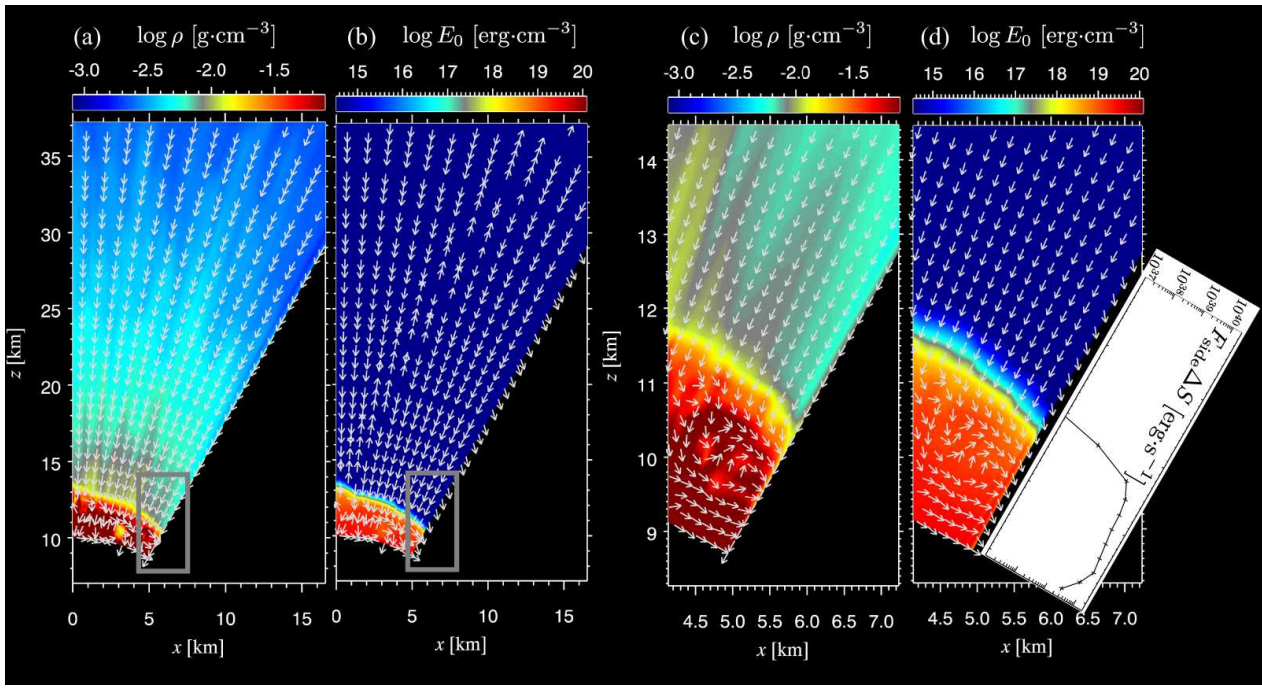


Fig. 1. Two-dimensional diagrams displaying mass and energy flow of super-critical column accretion at the elapsed time of 0.0335 sec. The left two panels show the structure of a column within $r = 37$ km, whereas the right two are magnified views of the innermost region enclosed by the gray squares in the left ones. In each pair of panels, the left panels show matter density color contours overlaid with matter velocity, while the right ones show color contours of radiation energy density overlaid with radiation flux in the laboratory frame (i.e., $\mathbf{F}_0 + \mathbf{v}E_0$), respectively. Radial profile of the radiation luminosity leaked from the side of accreting column with an area of $\Delta S \equiv 2\pi r \sin \theta \Delta r$ is shown in the inserted figure, where $\Delta r \sim 0.2$ km is the mesh spacing.

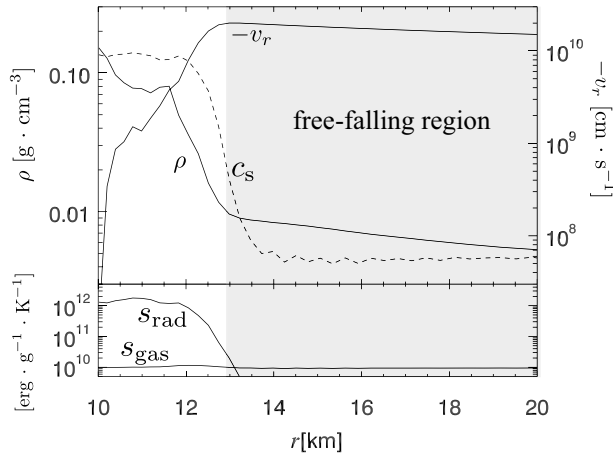


Fig. 2. (Top) Azimuthally averaged radial profile of the matter density and the velocity at the elapsed time of $t = 0.0335$ sec. Each quantity is averaged in the θ direction, e.g., $2\pi \int_0^{\theta_{\text{out}}} \rho r^2 \sin \theta d\theta / (2\pi \int_0^{\theta_{\text{out}}} r^2 \sin \theta d\theta)$. A weak shock formed at $r \sim 13$ km separates the upper, nearly free-fall region (shaded region) and the settling region, in which gas is drastically decelerated by the radiation pressure and matter is thus being accumulated. (Bottom) Same as the top panel but for gas entropy and radiation entropy.

indicates that the radiation gains entropy from gas and loses entropy by outgoing radiation at similar rates.

We have so far confirmed that super-critical accretion ac-

tually occurs through the accretion column. The next issue is to clarify how it occurs despite huge radiation energy density accumulating on the NS surface. For this purpose, we examine how the energy conversion occurs from gas to radiation by using figure 3. Here, the plotted quantities are either of volume-integrated energy density or surface-integrated energy flux density defined as: $\int q dV \equiv 2\pi \int_r^{\bar{r}} \int_{\theta_{\text{in}}}^{\theta_{\text{out}}} q r^2 \sin \theta dr d\theta$, and $\int F_q dS \equiv 2\pi \int_r^{\bar{r}} F_q \sin \theta_{\text{out}} r dr$, where q is energy density, F_q is energy flux density and integration is made from radius r to $\bar{r} = 50$ km. The selected quantities are gravitational energy (q_{grav}), advection energy of gas ($q_{\text{adv}}^{\text{gas}}$), time derivative of gas energy density ($\partial e_{\text{gas}}/\partial t$), radiation energy density converted from gas (with two different expressions, $q'_{(\text{gas} \rightarrow \text{rad})}$ and $q_{(\text{gas} \rightarrow \text{rad})}$), time derivative of radiation energy density ($\partial E_0/\partial t$), advection energy of radiation ($q_{\text{adv}}^{\text{rad}}$), and radiation energy flux density emitted from the unit area of the side wall (F_{side}), respectively, where $q_{\text{grav}} \equiv -GMv_r/(r-r_s)^2$, $q_{\text{adv}}^{\text{gas}} \equiv \nabla \cdot (\rho v^2 \mathbf{v}/2 + \gamma e \mathbf{v})$, $e_{\text{gas}} \equiv \rho v^2/2 + e$, $q'_{(\text{gas} \rightarrow \text{rad})} \equiv 4\pi \kappa B - c\kappa E_0 + (\chi/c) \mathbf{F}_0 \cdot \mathbf{v}$, $q_{(\text{gas} \rightarrow \text{rad})} \equiv 4\pi \kappa B - c\kappa E_0 + \nabla \mathbf{v} : \mathbf{P}_0$, and $q_{\text{adv}}^{\text{rad}} \equiv \nabla \cdot (\mathbf{v} E_0)$, respectively.

Let us first see how gas energy changes its form in the upper panel of figure 3. As gas falls down, the gravitational energy is gradually released (see the line labeled with $\int q_{\text{grav}} dV$). However, the sum of the liberated energy and the advection energy is kept nearly constant until gas reaches the accretion

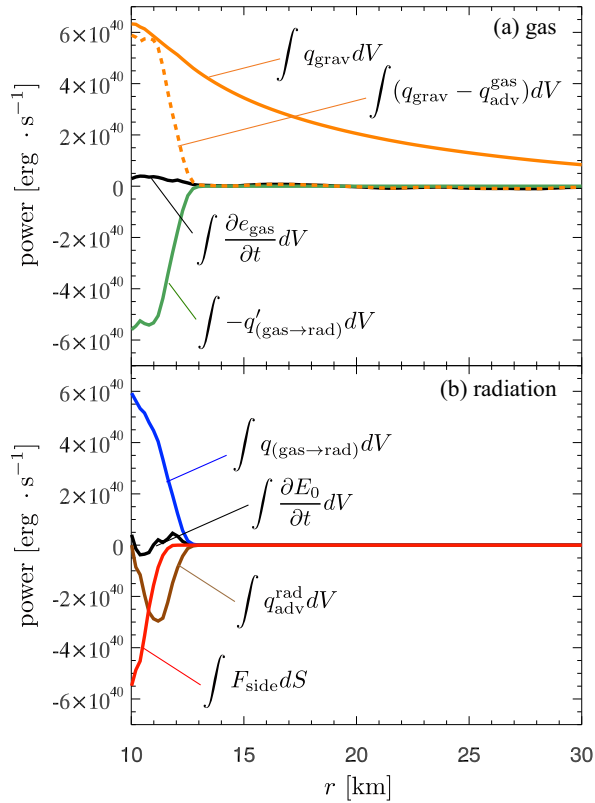


Fig. 3. Radial distributions of energy density forms of gas (upper panel) and of radiation (lower panel), respectively. The elapsed time is $t = 0.0335$ sec.

at $r_{\text{shock}} \sim 13$ km, meaning that all the liberated energy is carried downward by the falling gas. Since photons near the NS push the plasma outward, falling gas is suddenly decelerated at the shock surface. Below the shock surface, a part of the liberated energy is converted to radiation energy (see the line labeled with $\int -q'_{(\text{gas} \rightarrow \text{rad})} dV$). As a result, the gas energy e_{gas} is kept nearly constant in time, which guarantees the existence of stationary flow.

Let us next see how radiation energy changes its form in the lower panel of figure 3. As mentioned above, gas energy is converted to radiation energy below r_{shock} (see the line labeled with $\int q_{(\text{gas} \rightarrow \text{rad})} dV$). Nearly the same amount of energy is radiated away through the side boundary (see the line labeled with $\int F_{\text{side}} dS$). That is, the converted energy to radiation is carried to the side boundary and is radiated away at a similar height. We note, however, that the time derivative of the radiation energy density ($\partial E_0 / \partial t$) is non-zero below r_{shock} and is nearly balanced with the advection of radiation energy. This occurs because of convective motion of radiation bubbles [see circulating vectors in fig. 1 (c) and (d)].

The matter under the shock slowly accretes onto the NS, and emit the photons, whose luminosity is nearly Eddington luminosity. We note that isotropic luminosity at the NS sur-

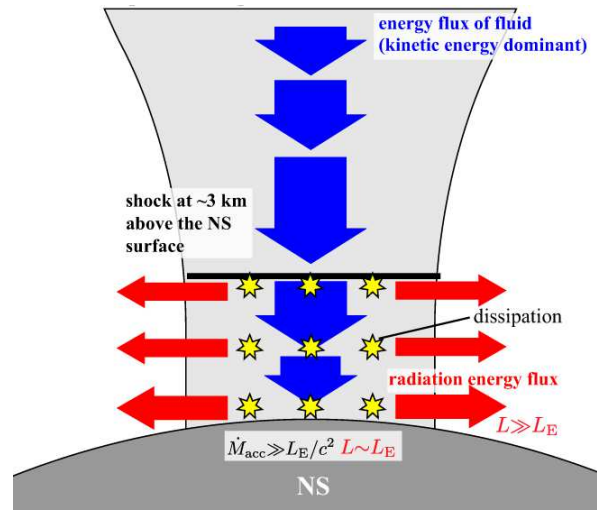


Fig. 4. Schematic picture explaining energy flow from gas (potential energy) to outgoing radiation within a super-critical accretion column. The blue arrows represent the energy flow carried by gas; their length and width are drawn in proportional to the kinetic energy flux and the mass accretion rates, respectively, whereas the red arrows represent energy flow carried by radiation and their widths are drawn in proportional to the radiation energy flux.

face is $\sim 3L_E$, which can be obtained by multiplying the luminosity at the NS surface within the accretion column $2\pi \int_0^{\theta_{\text{out}}} F_0^r(r_{\text{in}}, \theta) r^2 \sin \theta d\theta$ by the correction factor $4\pi/\Omega$. This isotropic luminosity is consistent with that of Ohsuga (2007).

4 Discussion

In this *letter* we study the two dimensional structure of a narrow super-critical accretion column with radiation transfer by means of the axisymmetric radiation hydrodynamic simulation. The accretion column is composed of an upper, free-fall region and a lower settling region with a shock being formed at the interface. Gas energy is converted to radiation only below the shock surface, and it is finally radiated away from the side surface. Super-Eddington luminosity is produced there, while nearly Eddington luminosity is emitted from the NS surface. Such basic energy flow is summarized in figure 4.

There are similarities and differences among three super-critical accretion systems (see table 1). The most distinctive features are found in the final form of energy; that is, it differs among them how excess energy can be taken away from the central engine at a rate exceeding the classical Eddington limit. Excess energy is carried by trapped photons in the black hole disk accretion, by outflow material in the form of its kinetic energy in disk accretion onto a non-magnetized NS (Ohsuga 2007), and by outgoing radiation emitted from the side boundary in column accretion onto a magnetized NS. In any case the outward flux measured in the laboratory frame ($F_0 + vE_0$) is much reduced in the innermost part of accretion flow. This con-

dition makes super-critical accretion feasible.

Since most of excess energy is finally radiated away from the side boundary in the magnetized NS case, strong electromagnetic radiation should be finally observed, unlike other two cases. The most unique feature of the ULX-pulsar is highly anisotropic radiation fields. This occurs, since large luminosity radiation goes out through the side boundary and not from the top of the accretion column. If the rotation axis and the magnetic axis of the NS do not coincide, we thus expect pulsed emission to be observed.

In the present study, we observe circulating gas motion in the settling region (see figure 1). Such motion affects energy transport processes and is described by the photon advection term in our analysis (see the bottom panel of figure 3). Such gas motion, known as ‘‘photon bubbles’’, was intensively studied by Klein & Arons (1989) by means of the RHD simulations. They carefully solve the super-Eddington atmosphere on the magnetized NS and found strong radiation-driven, optically thin outflow embedded in optically thick, inflowing plasma. They estimated that the growth timescale of such photon bubbles are is on the order of a millisecond. They also observe rapid time variability on millisecond timescales. Arons (1992) made the linear analysis, finding that the growth time is inversely proportional to the wavenumber, thereby concluding that the layer is eventually dominated by a few large bubbles. These features are in good agreement with our results.

Despite the existence of internal gas circulation, the fractional luminosity $F_{\text{side}}\Delta S$ is remarkably uniform except in the innermost region and thus seems not to be affected by photon bubbles [see the inserted figure next to figure 1(d)]. The photon bubbles are time-dependent, thus photon advection directly leads to time changes of radiation energy density (see the bottom panel of figure 3). Such time dependence is smoothed on long terms and, hence, does not affect the fractional luminosity profile.

In the present study, we assume that magnetic fields are not so strong so that the two-dimensional gas motion can be allowed within the column. That is, in our model, both of radiation-pressure and ram-pressure forces are comparable to the Lorentz force and transport the radiative energy by the advection, while the accretion column is possibly sustained due to marginally strong Lorentz force at the side surface of the column. By using our simulation data, this marginal B-field strength inside the column can be estimated to be $\sim 10^{10}\text{G}$, which is not anomalous in pulsars. The perfect confinement of the column may look

slightly difficult to be sustained, since the radiative force can dominate the Lorentz force with the marginal magnetic fields at the side wall. However, the column accretions as shown in our simulation should be still feasible for the following two reasons: (1) The magnetic fields inside the column will be pushed towards the side wall due to the fluid motion with the frozen-in magnetic fields, leading to accumulation of the B-field at the column side. Then the enhanced magnetic tension force and magnetic pressure gradient force can overcome the radiative force. (2) Even if the perfect confinement of the column is not sustained, the mass loss due to radiative force in the θ -direction at the side wall cannot significantly change our result, since the sound speed of the radiation dominated gas at the side surface is $\sim 10\%$ of the accretion velocity, indicating that the mass loss rate through the column side will only be $\sim 10\%$, at maximum, of mass accretion rate. We plan to explore as future work the cases of much stronger magnetic fields which forbid the fluid motions perpendicular to the magnetic field (i.e., the θ -direction).

Here, we discuss the location of the photosphere. In the r -direction, the scattering photosphere and the effective photosphere appear at $\sim 0.03\text{ km}$ and $\sim 100\text{ km}$, respectively, inside from the outer boundary ($r_{\text{out}} \sim 2000\text{ km}$). Both of them are thus located far outside the shock surface ($r_{\text{shock}} \sim 13\text{ km}$). In the θ -direction, the scattering photosphere is at around $\sim 10^{-4}\text{ km}$ from the side boundary at $r \sim 12\text{ km} (< r_{\text{shock}})$. Although the column is effectively optically thin ($\tau_{\text{eff}} \sim 0.03$) at $r \sim 12\text{ km}$ if the gas temperature is kept high, the effective optical depth is more likely to be $\tau_{\text{eff}} \simeq 10$ if Comptonization is properly taken into account; that is, the matter temperature will then be much cooler $\sim 10^8\text{ K}$ (i.e., gas temperature will decrease to radiation temperature via the Comptonization). That is, the effective photosphere will appear around 0.5 km from the side wall, if the gas is strongly Comptonized. The Comptonization timescale is, in fact, much shorter than the accretion timescale as briefly discussed below.

In the present study, we rather simplified the physical situation to focus on the basic observational features of the super-critical accretion column, thus omitting some potentially important physical processes. For example, we ignored thermal Compton scattering, which could be of great importance when considering detailed radiation spectra (Kawashima et al. 2009, 2012) because the plasma is scattering dominant and gas temperature is much greater than radiation temperature under the shock surface. (We note that the fluid dynamics found in this *letter* will not be significantly affected by the Comptonization as described below.) At first, we show the importance of the Comptonization to determine gas temperature distribution, and then, we present the reason why the dynamics will not be significantly modified by the Comptonization. Under the shock surface, gas temperature is orders of magni-

Table 1. Three classes of super-critical accretion systems

central object	photon luminosity	final energy carrier
black hole	$\gtrsim L_{\text{E}}$	trapped photons
non-magnetized NS	$\sim L_{\text{E}}$	outflow (kinetic energy)
magnetized NS	$\gg L_{\text{E}}(\Omega/4\pi)$	outgoing radiation

tude higher than radiation temperature. The Comptonization, which relaxes the gas and radiation temperature, will sufficiently change the gas temperature distribution, because the estimated Comptonization timescale ($\sim 10^{-11}$ s) is by seven orders of magnitude shorter than the accretion timescale ($\sim 10^{-4}$ s). Here, the Comptonization timescale is estimated by using the Compton cooling rate based on the Kompaneets equation (see, e.g. the equation (3) in Kawashima et al. 2009), substituting gas temperature $\sim 10^{10}$ K, radiation temperature $\sim 10^8$ K, and mass density $\sim 10^{-1.5} \text{g cm}^{-3}$. Thus, we can expect that the gas temperature will significantly decrease due to the Comptonization. Despite the importance of the Compton scattering, we can expect that the dynamics of the flow will not be significantly changed by the Comptonization. This is because the flow dynamics is governed by the radiative force and the radiation energy density is 1-3 orders of magnitude larger than the gas internal energy density below the shock surface, which indicates that the increment of the radiation energy converted from the gas internal energy via the Comptonization is too small to significantly change the dynamics of the accretion column. The Comptonization may be, therefore, important only when we calculate the spectra of the accreting column: we expect that a modified-blackbody spectrum with a Wien peak will be formed, since the accretion column is scattering dominant and the Compton y -parameter is much greater than unity under the shock surface. In this *letter*, three dimensional gas motion (due to the NS rotation, etc.) is also ignored. Further, we used the FLD approximation for solving radiation transfer, which need to be improved. We also simplify the plasma processes near the NS; that is, we have not considered neutrino emission nor included corrections to hydrodynamics and radiative transport due to strong magnetic fields (Klein & Arons 1989). These effects will be explored in a next paper.

Acknowledgments

We thank H.R. Takahashi for useful discussion. The numerical simulations were carried out on the XC30 at the Center for Computational Astrophysics, National Astronomical Observatory of Japan. This work is supported in part by Grants-in-Aid of the Ministry of Education, Culture, Sports, Science and Technology (MEXT) (26400229, S.M.; 15K05036, K.O.). This work was supported in part by MEXT HPCI STRATEGIC PROGRAM and the Center for the Promotion of Integrated Sciences (CPIS) of Sokendai, and MEXT as a priority issue (Elucidation of the fundamental laws and evolution of the universe) to be tackled by using post-K Computer and JICFuS.

References

- Arons, J. 1992, *ApJ*, 388, 561
 Bachetti, M., Harrison, F. A., Walton, D. J., et al. 2014, *Nature*, 514, 202
 Basko, M. M., & Sunyaev, R. A. 1976, *MNRAS*, 175, 395
 Begelman, M. C. 1978, *MNRAS*, 184, 53
 Colbert, E. J. M., & Mushotzky, R. F. 1999, *ApJ*, 519, 89
 Colella, P., & Woodward, P. R. 1984, *Journal of Computational Physics*, 54, 174
 Fabbiano, G. 1989, *ARA&A*, 27, 87
 Feng, H., & Soria, R. 2011, *New A Rev.*, 55, 166
 Kawashima, T., Ohsuga, K., Mineshige, S., et al. 2009, *PASJ*, 61, 769
 —. 2012, *ApJ*, 752, 18
 King, A. R., Davies, M. B., Ward, M. J., Fabbiano, G., & Elvis, M. 2001, *ApJ*, 552, L109
 Klein, R. I., & Arons, J. 1989, in *ESA Special Publication*, Vol. 296, Two Topics in X-Ray Astronomy, Volume 1: X Ray Binaries. Volume 2: AGN and the X Ray Background, ed. J. Hunt & B. Battrick
 Levermore, C. D., & Pomraning, G. C. 1981, *ApJ*, 248, 321
 Makishima, K., Kubota, A., Mizuno, T., et al. 2000, *ApJ*, 535, 632
 Ohsuga, K. 2007, *PASJ*, 59, 1033
 Ohsuga, K., Mori, M., Nakamoto, T., & Mineshige, S. 2005, *ApJ*, 628, 368
 Paczyński, B., & Wiita, P. J. 1980, *A&A*, 88, 23
 Soria, R. 2007, *Ap&SS*, 311, 213
 Turner, N. J., & Stone, J. M. 2001, *ApJS*, 135, 95
 Vierdayanti, K., Mineshige, S., Ebisawa, K., & Kawaguchi, T. 2006, *PASJ*, 58, 915
 Watarai, K., Mizuno, T., & Mineshige, S. 2001, *ApJ*, 549, L77